RSC Advances

PAPER

View Article Online
View Journal | View Issue



Cite this: *RSC Adv.*, 2023, **13**, 4532

# Microporous carbon for fast and simple electrochemical detection of imidacloprid insecticide in fruit and water samples†

Keerakit Kaewket and Kamonwad Ngamchuea *

Received 10th January 2023
Accepted 27th January 2023

DOI: 10.1039/d3ra00192j

rsc.li/rsc-advances

Herein, a fast and sensitive electrochemical sensor was developed for imidacloprid detection using low-cost disposable microporous carbon screen-printed electrodes. The electrochemical behaviour of imidacloprid at the microporous material was investigated in detail. The developed sensor allowed imidacloprid detection in the linear range of 0.00–1.00 mM with a sensitivity of 14.43 ± 0.42 μA $mM^{-1}$ and a detection limit of 2.54 μM ($3s_B/m$). The sensor showed excellent selectivity and high tolerance to possible interference from other tested insecticides and ions. Excellent repeatability (3.42%, $n = 3$) and reproducibility (2.23%, $n = 3$) were demonstrated. Application of the sensor in various fruit and water samples without any treatment showed 96.2–103.0% recoveries. The developed sensor further revealed that the most effective method for removing imidacloprid residue from fruit samples was *via* washing with a mixture of 5% w/v NaCl and 5% w/v bicarbonate at 40 °C.



## 1 Introduction

Since their introduction in the early 1990s, neonicotinoids have become the most widely used insecticides in the world.[1] Compared with organochlorines and organophosphates, neonicotinoids have relatively low toxicity for mammals. Imidacloprid (1-((6-chloro-3-pyridinyl) methyl)-*N*-nitro-2-imidazolidnimine or IMP, refer to Fig. 1) is one of the most commonly used neonicotinoid insecticides. Imidacloprid consists of a 6-chloro-3-pyridyl moiety which can selectively damage the insects' central nervous system.[2] Imidacloprid can be applied *via* foliar spraying, seed dressing, and soil treatment to protect crops from insect pests.

However, the rapidly increasing use of imidacloprid in recent years has led to negative impacts on non-target organisms and ecosystems. The systemic nature of imidacloprid causes the compound to be distributed to different parts of the plant such as pollen, nectar, and guttation fluids, inducing negative effects on beneficial insects such as bees, pollinators, and honey providers. Imidacloprid is chemically stable under neutral and acidic conditions,[3] which means that the compound can accumulate in the soil. Its water solubility also means that imidacloprid is prone to leaching into water resources.

In recent years, there have been several reports on imidacloprid contamination in soil, water, and several plants such as apple, rice, tomato, corn, and grapevine.[4] The concentration of imidacloprid in urine has also been found to significantly increase in farmers.[5] The USA National Health and Nutrition Examination Survey further reported that young children and Asians may be exposed to higher levels of imidacloprid than other age and ethnic groups.[6] Exposure to imidacloprid may lead to severe respiratory failure, severe gastrointestinal symptoms, unconsciousness, lymphocyte apoptosis, and neuropsychiatric characteristics.[7] The use of imidacloprid on outdoor crops has been banned by the European Union in 2018.[8] In many countries, however, the use of imidacloprid is still allowed and is widely popular among farmers.[9] There is thus an urgent need to develop a fast and facile sensor for IMP detection in food and environmental samples.

To date, imidacloprid can be detected by high-performance liquid chromatography-mass spectrometry,[10] gas chromatography-mass spectrometry,[11] surface plasmon resonance,[12] fluorescence,[13] chemiluminescence,[14] terahertz spectrometry,[15] and quartz crystal microbalance.[16] However, onsite

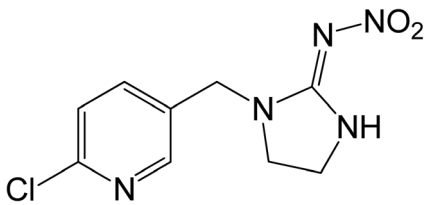


Fig. 1 Chemical structure of imidacloprid (IMP).

*School of Chemistry, Institute of Science, Suranaree University of Technology, 111 University Ave, Muang District, Nakhon Ratchasima, 30000, Thailand. E-mail: kamonwad@g.sut.ac.th; Tel: +66 44 224 637*

† Electronic supplementary information (ESI) available. See DOI: https://doi.org/10.1039/d3ra00192j

applications are often not possible with these techniques due to the complex instrumentation and sample preparation. As imidacloprid has a moiety that can undergo a reduction reaction in aqueous environment, simple electrochemical methods which can be operated by handheld device can thus provide fast, sensitive, and low-cost detection of imidacloprid.[17–29]

Herein, a fast and simple electrochemical sensor was developed for imidacloprid detection *via* the use of microporous carbon electrode. Microporous carbon is a low-cost material that is easy to manufacture, has high electrical conductivity, and large surface-to-volume ratio, which makes it an ideal material for electroanalytical applications.[30,31] Importantly, the employed microporous material provides advantages of the synergy between the enhanced electroactive surface area and the thin-layer behaviours within the microporous structure. The former improves the sensitivity of the electrochemical detection, while the latter lowers the required overpotential and helps with the selectivity of the measurement.

Miniaturization of the sensor was further performed by developing disposable microporous carbon modified screen-printed electrodes. The integrated three-electrode system on a substrate facilitated the use of the sensor for onsite applications and significantly reduced the amount of sample required for the analysis (*ca.* 50 μL). Application of the developed sensor in investigating the effects of fruit washing processes on the removal of imidacloprid residues was then further demonstrated in this work.

# 2 Experimental

## 2.1 Chemical reagents

All chemical reagents were of analytical grades and used as received without further purification: imidacloprid ($C_9H_{10}ClN_5O_2$, 98.0%, AK Scientific), potassium chloride (KCl, ⩾99.0%, Sigma-Aldrich), sodium citrate dihydrate ($C_6H_9Na_3O_9$, ⩾99.0%, Sigma-Aldrich), citric acid ($C_6H_8O_7$, 99.5%, QRëC), sodium phosphate dibasic ($Na_2HPO_4$, ⩾99.0%, Sigma-Aldrich), sodium phosphate monobasic ($NaH_2PO_4$, ⩾99.0%, Sigma-Aldrich), sodium bicarbonate ($NaHCO_3$, 99.7%, QRëC), sodium carbonate ($Na_2CO_3$, 99.5%, Kemaus), hydrochloric acid (HCl, 37%, QRëC), sodium hydroxide (NaOH, ⩾98.5%, Sigma-Aldrich), calcium chloride ($CaCl_2$, 99.9%, APS Ajax Finechem), sodium nitrite ($NaNO_2$, ⩾ 97.0%, Sigma-Aldrich), potassium iodide (KI, ⩾99.0%, Sigma-Aldrich), potassium bromide (KBr, ⩾99.0%, Sigma-Aldrich), ethion ($C_9H_{22}O_4P_2S_4$, Bharat Rasayan Limited), dichlorvos ($C_4H_7Cl_2O_4P$, 50.0%, Extra Agrochemical), and indoxacarb ($C_{22}H_{17}ClF_3N_3O_7$, 15.0%, AG-GRO), carbendazim ($C_9H_9N_3O_2$, 50.0%, Amax Inter). Commercial microporous carbon was obtained from IRPC Public Company Limited, Thailand.

## 2.2 Electrochemical studies

Electrochemical experiments were performed with an Autolab PGSTAT302N potentiostat (Metrohm, Netherlands) using a standard three-electrode setup thermostated at 25 °C in a Faraday cage. A bare glassy carbon electrode (GCE, 3.0 mm diameter, ItalSens, Netherlands), a microporous carbon modified glassy carbon electrode (MC/GCE), or a microporous carbon modified screen-printed carbon electrode (MC/SPE) was employed as a working electrode. A silver/silver chloride (Ag/AgCl in 3.4 M KCl, ItalSens, Netherlands) and a platinum sheet (ItalSens, Netherlands) were used as reference and counter electrodes, respectively.

Prior to use, the GCE was polished on a water–alumina slurry (1.0 μm, 0.3 μm and 0.05 μm, Buehler, USA) on soft lapping pads (Buehler, USA). The modification with microporous carbon was achieved by preparing the suspension of 1.0 mg of microporous carbon in 1.0 mL deionized water and sonicated for 60 minutes to disperse the material. Afterwards, 6 μL of the suspension was dropcasted on either the freshly polished GCE or the graphite screen-printed electrode (SPE, 3.0 mm diameter working electrode, ItalSens IS-C, Netherlands). The electrodes were left to dry at 50 °C in an oven for 10 minutes. The detail of the characterization of microporous carbon has been fully described in our previous work.[32,33]

Electrochemical measurements were performed in the presence of buffers pH 3.0 (citrate buffer), pH 5.0 (citrate buffer), pH 7.0 (phosphate buffer, PBS), pH 9.0 (carbonate buffer) or pH 11.0 (carbonate buffer). The ionic strengths of all solutions were adjusted to 0.10 M by the addition of potassium chloride (KCl).

## 2.3 Application to real samples

The developed method was validated by spiking and recovery tests (standard addition) in various fruit and water samples. The fruit samples (orange, lime, tomato, and watermelon) were purchased from the local supermarket (Nakhon Ratchasima, Thailand). All fruit samples were washed thoroughly with water. The juice was then obtained by squeezing and filtered to remove solid particles. Tap water (Suranaree University of Technology, Thailand) and reservoir water (Sura Reservoir, Thailand) were collected and used without further sample treatment. The samples which were diluted 10-fold in phosphate buffer (0.10 M PBS pH 7.0) and spiked with IMP were subjected to DPV measurements at a microporous carbon modified screen-printed carbon electrode (MC/SPE) at the pulse amplitude of 0.15 V, the pulse width of 0.05 s, and the pulse period of 0.5 s. The obtained results were then analyzed and reported as percentage recoveries.

## 2.4 Evaluation of fruit washing processes in imidacloprid removal

The develop sensor was then applied to determine the amounts of IMP residues in tomato samples, which were washed by different solvents at different temperatures. First, the tomatoes were soaked in commercial IMP insecticide (0.5 g $L^{-1}$) for 1.5 hours. The tomatoes were then washed for 1 minute with tap water or other common solutions used in fruit cleaning such as 2% w/v sodium chloride, 5% w/v sodium chloride, 5% w/v sodium bicarbonate, and a mixture of 5% w/v sodium chloride and 5% w/v sodium bicarbonate. The effects of temperature

were also investigated at 5 °C, 25 °C, and 40 °C. The samples were then prepared according to Section 2.3 for IMP analysis.

# 3 Results and discussion

First, the electrochemical properties of imidacloprid (IMP) were investigated at a bare glassy carbon electrode (GCE) and a microporous carbon modified glassy carbon electrode (MC/GCE). The measuring conditions such as pH, scan rates, and the amount of deposited microporous carbon were optimized. The developed sensor was then miniaturized *via* the use of a microporous carbon modified screen-printed electrode (MC/SPE). Finally, the sensor was validated and applied to detect IMP in fruit and water samples.

## 3.1 Electrode characterization

The electroactive surface areas of the electrodes were determined by cyclic voltammetry in the solution of 1.0 mM hexaammineruthenium(III) ($[Ru(NH_3)_6]^{3+}$ or RuHex), which is a standard outer-sphere redox probe, in the presence of 0.10 M KCl supporting electrolyte at varied scan rates. The electroactive surface areas were then analyzed according to the Randles–Sevcik equation for an electrochemically reversible one-electron transfer process (eqn (1)) to be $6.65 \times 10^{-6} \pm 0.04 \times 10^{-6}$ m$^2$ and $1.08 \times 10^{-5} \pm 0.02 \times 10^{-5}$ m$^2$ for a bare GCE and MC/GCE, respectively.[34]

$$I_p = 0.446FAc^*\sqrt{\frac{FDv}{RT}}, \quad (1)$$

where $I_p$ is the peak current, $F$ is the Faraday's constant (96 485 C mol$^{-1}$), $A$ is the electroactive surface area, $c^*$ is the bulk concentration of $[Ru(NH_3)_6]^{3+}$, $v$ is the voltage scan rate (V s$^{-1}$), $R$ is the molar gas constant (8.314 J K$^{-1}$ mol$^{-1}$), $T$ is the absolute temperature (K), and $D$ is the diffusion coefficient of $[Ru(NH_3)_6]^{3+}$ ($8.61 \times 10^{-10} \pm 0.06 \times 10^{-10}$ m$^2$ s$^{-1}$).[33]

Electrochemical impedance spectroscopy (EIS) was next performed in the solution of 1.0 mM $Fe(CN)_6^{3-/4-}$ and 0.10 M KCl in the frequency range of 1–10$^5$ Hz, and the amplitude of

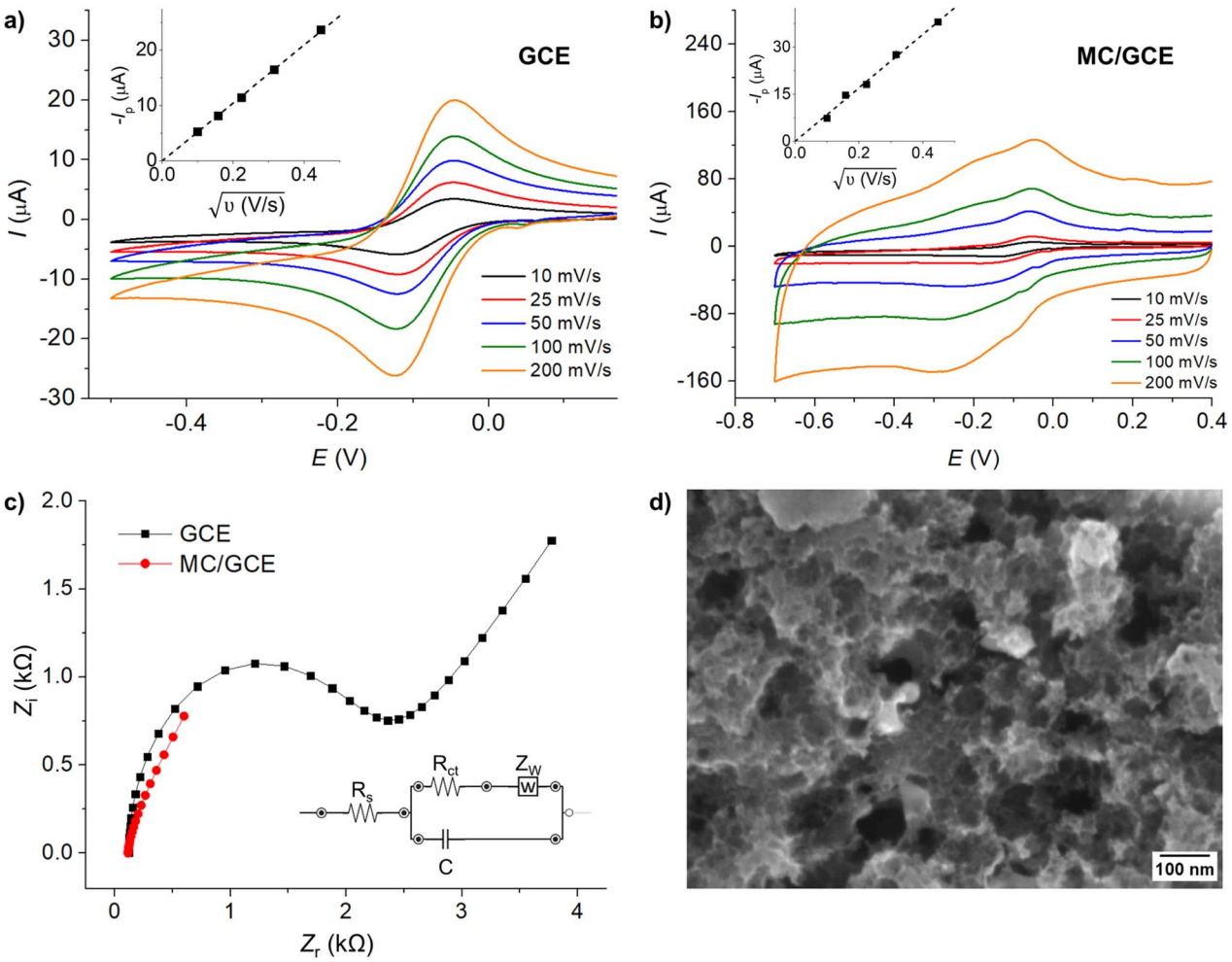


Fig. 2 Cyclic voltammetry of 1.0 mM $[Ru(NH_3)_6]^{3+}$ in 0.10 M KCl at (a) bare GCE and (b) MC/GCE at varied scan rates. The inlays show the plots of peak currents ($I_p$) *vs.* square root of scan rates ($\sqrt{v}$). The data points and error bars represent the mean values and standard deviation ($n = 3$), respectively. (c) EIS spectra of bare GCE *vs.* MC/GCE in 1.0 mM $Fe(CN)_6^{3-/4-}$ and 0.10 M KCl in the frequency range of 1–10$^5$ Hz, and the amplitude of 5 mV. (d) SEM image of microporous carbon.

5 mV at bare GCE and MC/GCE (Fig. 2c). The data were fitted with a Randles circuit model (Fig. 2c, inlay). The charge transfer resistances ($R_{ct}$) of GCE and MC/GCE were determined to be 2.28 ± 0.29 kΩ and 0.013 ± 0.007 Ω, respectively. The double layer capacitances ($C_{dl}$) of GCE and MC/GCE were 0.56 ± 0.05 μF and 78.8 ± 1.4 μF, respectively. The high double layer capacitance of MC/GCE was consistent with its large electroactive surface area. The relatively low charge transfer resistance of microporous carbon has become one of its advantages for application in electrochemical sensors.

The pore size and surface functional groups on microporous carbon had been fully characterized in our previous work.[32,33] The size of the pores was 1.89 nm diameter on average and the specific surface area was 1270 $m^2$ $g^{-1}$ according to the Brunauer–Emmett–Teller (BET) model measured using the nitrogen adsorption–desorption isotherm. Fourier-transform infrared spectroscopy (FT-IR) revealed the presence of O–H, C=O, C=C, C–O, and C–C functional groups on the surface of microporous carbon which may interact with IMP through H-bonding and dipole–dipole attraction.

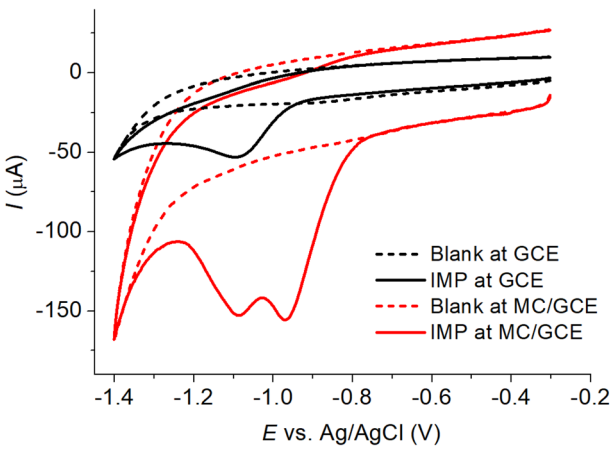


Fig. 3 Cyclic voltammetry of (solid lines) 0.60 mM imidacloprid (IMP) in PBS pH 7.0 or (dashed lines) blank PBS pH 7.0 at the scan rate of 50 mV $s^{-1}$ at (black) bare GCE and (red) MC/GCE.

### 3.2 Cyclic voltammetry of IMP at GCE *vs.* MC/GCE

At a bare GCE, a reduction peak of IMP in PBS buffer pH 7.0 was observed at −1.09 V (Fig. 3). At an MC/GCE, the peak current was enhanced by *ca.* 200% (*cf.* bare GCE) due to the increased electroactive surface area. At an MC/GCE, another peak appeared at lower overpotential ($E_p$ = −0.97 V) in addition to the peak at −1.09 V (Fig. 3). The splitting of the peaks at an MC/GCE occurred due to the change of mass transfer mode from exclusively *planar diffusion* at a bare GCE to mixed diffusion regimes at the porous MC/GCE consisting of *planar diffusion* ($E_p$ = −1.09 V) and *thin-layer diffusion* ($E_p$ = −0.97 V *i.e.* at lower overpotentials).[35,36] This type of peak splitting was often observed in systems with irreversible electrode kinetics.[35,36] The absence of the backward peaks at both electrodes suggested that the reduction of IMP was chemically irreversible in the timescale of the experiment with the formation of either an unstable product or a product which is not electroactive.

### 3.3 Tafel analysis

The currents in the range of 15–50% of the peak currents of the voltammograms at the slow scan rate of 10 mV $s^{-1}$ were subjected to Tafel analysis (eqn (2)).[37,38] The employed current range and the slow scan rate were chosen to avoid the influence of diffusional mass transport.

$$\frac{\partial \ln I}{\partial E} = \frac{-(n' + \alpha_{n'+1})F}{RT}, \quad (2)$$

where $I$ is the electrical current, and $E$ is the applied potential. $n'$ is the number of electrons transferred before the rate determining electron transfer step, $\alpha_{n'+1}$ is the cathodic transfer coefficient of the rate determining electron transfer step, $R$ is the molar gas constant (8.314 J $K^{-1}$ $mol^{-1}$), $T$ is the absolute temperature (K), and $F$ is the Faraday constant (96 485 C $mol^{-1}$).[39]

According to Fig. 4, the values of $n' + \alpha_{n'+1}$ were determined to be 0.63 ± 0.01 and 0.50 ± 0.01 at bare GCE and MC/GCE, respectively. The results thus indicated that the first electron transfer was the rate-determining step ($n' = 0$).

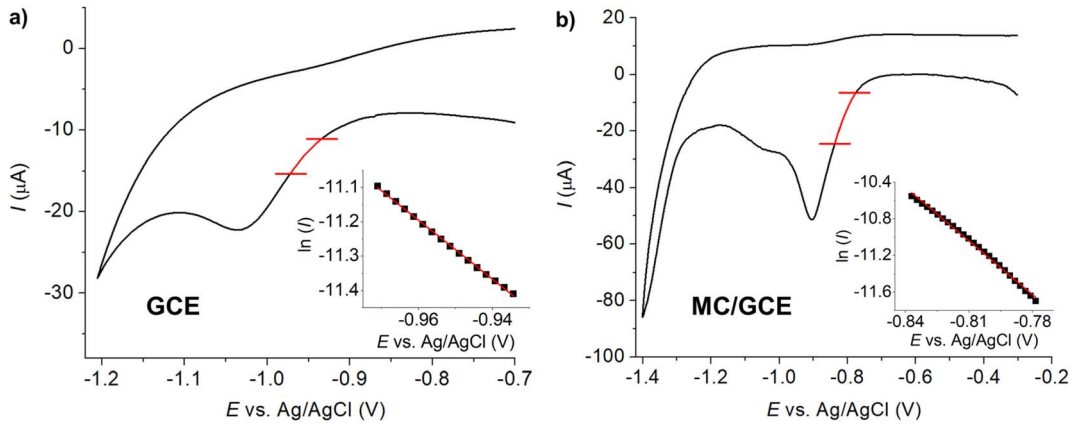


Fig. 4 Tafel analysis of 0.60 mM imidacloprid (IMP) in PBS pH 7.0 at the scan rate of 10 mV $s^{-1}$ at (a) bare GCE and (b) MC/GCE.

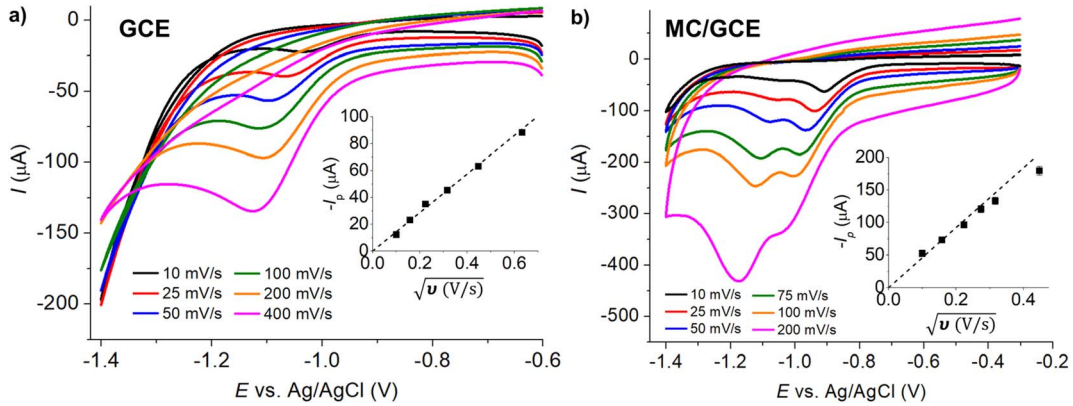


Fig. 5 Cyclic voltammetry at varied scan rates of 0.60 mM imidacloprid (IMP) in PBS pH 7.0 at (a) bare GCE and (b) MC/GCE. The inlays show the plots of peak currents ($I_p$) *vs.* square root of scan rates ($\sqrt{\nu}$). The data points and error bars represent the mean values and standard deviation ($n$ = 3), respectively.

Note that the shape of the two reduction peaks at MC/GCE in Fig. 4b are different from those in Fig. 3 due to the effect of scan rates which will be further discussed in the next section.

### 3.4 Effects of scan rates

Fig. 5 demonstrates the voltammograms of IMP at varied scan rates. The peak currents ($I_p$) increased linearly with the square root of scan rates ($\sqrt{\nu}$) at both bare GCE and MC/GCE, indicating diffusion-controlled processes at both types of electrodes.

The diffusion coefficient ($D$) of IMP was determined from peak currents at the bare GCE to be $1.3 \times 10^{-9} \pm 0.01 \times 10^{-9}$ m$^2$ s$^{-1}$ (*cf.* literature value = $1.6 \times 10^{-9}$ m$^2$ s$^{-1}$)[40] according to eqn (3) for an electrochemically irreversible process (slow electrode kinetics):[37]

$$I_p = (2.99 \times 10^5) Ac^* n \sqrt{D\nu(n' + \alpha_{n'+1})}, \quad (3)$$

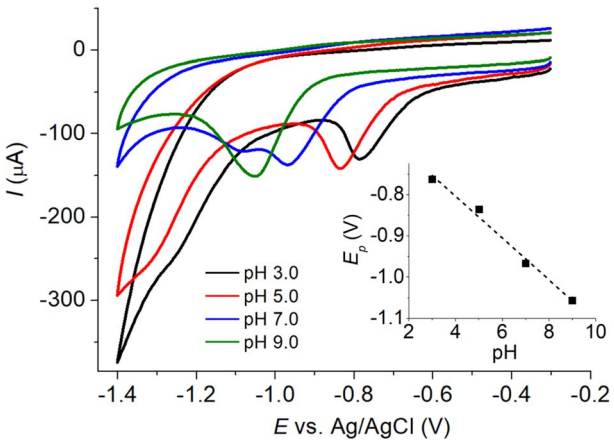


Fig. 6 Cyclic voltammetry at varied pH of 0.60 mM imidacloprid (IMP) at MC/GCE at the scan rate of 50 mV s$^{-1}$. The inlay shows the plot of cathodic peak potentials ($E_p$) against pH. The data points and error bars represent the mean values and standard deviation ($n$ = 3), respectively.

given that $\alpha_{n'+1} = 0.63 \pm 0.01$ (from Tafel analysis), $n'$ is the number of electrons transferred before the rate determining electron transfer step ($n' = 0$), $n$ is the total number of electrons transferred ($n = 4$),[40] $A$ is the electrode surface area, and $c^*$ is the bulk concentration of IMP ($c^*$ = 0.60 mM).

At MC/GCE, the ratios of the two cathodic peaks ($I_{p,\ -0.97\ V}/I_{p,\ -1.09\ V}$) changed with scan rates with the peak at lower overpotential (−0.97 V) dominant at slow scan rates. The peak at higher overpotential (−1.09 V) became dominant at faster scan rates. The peak splitting at an MC/GCE is due to the interplay of mass transport phenomena and electrode kinetics.[41] The first peak at −0.97 V is a consequence of *thin-layer diffusion*, where a small volume of solution is trapped inside the pores and the analyte depleted on the timescale of the experiment. The following peak at higher overpotential is due to *planar diffusion* of the electroactive species from bulk solution to the electrode surface.

### 3.5 Effects of pH

The effect of pH on the voltammetric response of IMP was next investigated at MC/GCE electrodes in the pH range of 3.0–9.0 (Fig. 6). The cathodic peak potentials of IMP negatively shifted with increasing pH with the slope of $-50.6 \pm 3.7$ mV pH$^{-1}$, close to the theoretical Nernstian value for an $ne^-$ $nH^+$ process. The results thus indicate an equal number of proton(s) and electron(s) transfer in the IMP reduction, in accordance with the results reported for other carbon based electrodes such as carbon paste, graphene oxide, and multiwall carbon nanotube.[19,42]

### 3.6 Effects of the amount of microporous carbon

As a higher amount of microporous carbon was deposited on the electrode surface, the peak currents of IMP reduction increased due to an enhance in the electroactive surface area (Fig. 7). However, when the amount of microporous carbon exceeded 6 μg, the current responses of IMP reduction no longer increased with the amount deposited due to the slow diffusion of IMP within the thick layers of microporous carbon.[43] Further

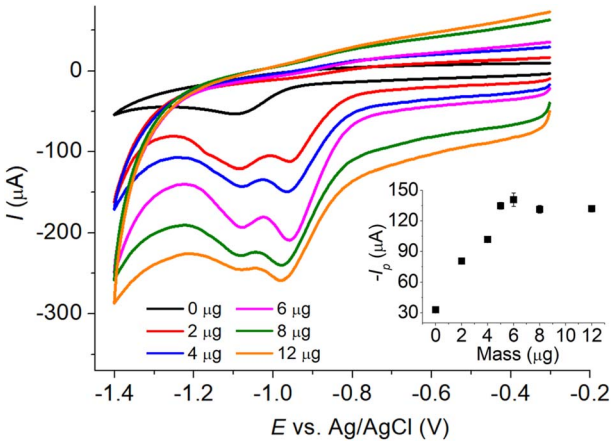


Fig. 7 Cyclic voltammetry of 0.60 mM imidacloprid (IMP) in PBS pH 7.0 at the scan rate of 50 mV $s^{-1}$ at MC/GCE deposited with different amounts of microporous carbon (MC). The inlay shows the plot of cathodic peak currents ($I_p$) *vs.* the amount of MC. The data points and error bars represent the mean values and standard deviation ($n = 3$), respectively.

increase in the amount of microporous carbon also caused the undesirable capacitive currents to be significantly large. The amount of microporous carbon of 6 μg was thus chosen for further analysis of IMP detection.

### 3.7 Calibration curves: CV

As the voltammetric responses of IMP at MC/GCE were significantly different at different scan rates, we evaluated the analytical performances at both slow (10 mV $s^{-1}$) and fast (200 mV $s^{-1}$) scan rates. Cyclic voltammograms of varied concentrations of IMP at MC/GCE are demonstrated in Fig. 8 with calibration curves provided in the inlays. At the scan rate of 10 mV $s^{-1}$, the linear range was 0.00–0.60 mM, the sensitivity was 83.7 ± 2.7 μA $mM^{-1}$, and the limit of detection ($3s_B/m$) was 3.22 μM (Fig. 8a). At the scan rate of 200 mV $s^{-1}$, the linear range, sensitivity, and limit of detection ($3s_B/m$) were determined to be 0.00–0.60 mM, 294.0 ± 5.8 μA $mM^{-1}$, and 6.61 μM, respectively (Fig. 8b). A lower limit of detection can thus be obtained at the slow scan rate for measurements using microporous carbon electrodes.

Note that when two peaks were observed in IMP reduction, the reported peak currents were determined from the peak at the lower overpotential.

### 3.8 Differential pulse voltammetry at disposable screen-printed electrodes

The analytical performance of the MC/GCE was next improved *via* the use of differential pulse voltammetry (DPV) to eliminate the capacitive background charging currents. The condition for DPV was optimized in Fig. S1, ESI.†

The sensor was further miniaturized *via* the use of screen-printed electrodes, which are easy to use, convenient, prevent cross-contamination of samples, and use a small volume of sample (*ca.* 50 μL). In this work, the graphite screen-printed electrodes were modified with microporous carbon by drop-casting (MC/SPE) and subjected to IMP measurements. The electrodes were characterized for their electroactive surface area (Fig. S2†) and charge transfer resistance (Fig. S3) in the ESI.† The electroactive surface area of bare SPE and MC/SPE were 7.41 × $10^{-6}$ ± 0.14 × $10^{-6}$ $m^2$ and 2.31 × $10^{-5}$ ± 0.11 × $10^{-5}$ $m^2$, respectively. The charge transfer resistances ($R_{ct}$) of SPE and MC/SPE were 16.9 ± 0.6 kΩ and 0.021 ± 0.009 Ω, respectively. We have further validated that $O_2$ reduction had no effect on the voltammetric response of IMP (result not shown). The detection of IMP can thus be performed directly at the microporous screen-printed electrodes (MC/SPE) without the need for deoxygenation.

Imidacloprid detection at the MC/SPE (Fig. 9) gave a linear relationship between peak currents and IMP concentrations in the range of 0.00–1.00 mM, the sensitivity of 14.43 ± 0.42 μA $mM^{-1}$, and the limit of detection of 2.54 μM ($3s_B/m$). Table 1 shows the comparison of the analytical performance of the developed sensor with those recently reported in the literature for the detection of IMP.

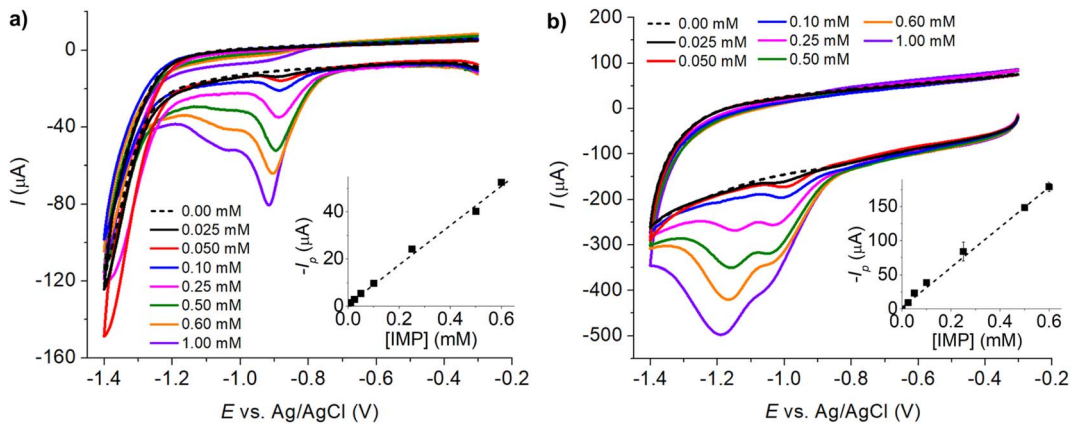


Fig. 8 Cyclic voltammetry of varied concentrations of imidacloprid (IMP) in PBS pH 7.0 at an MC/GCE at the scan rates of (a) 10 mV $s^{-1}$ and (b) 200 mV $s^{-1}$. The inlays show the calibration plots of peak currents ($-I_p$) *vs.* imidacloprid concentrations ([IMP]). The data points and error bars represent the mean values and standard deviation ($n = 3$), respectively.

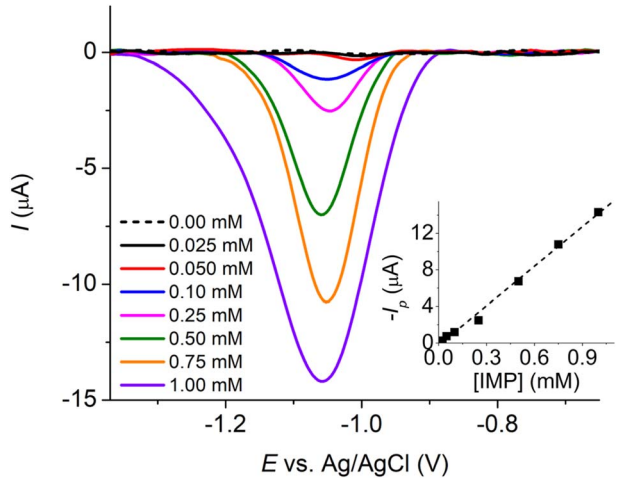


Fig. 9 Differential pulse voltammetry at microporous carbon screen-printed electrodes (MC/SPE) of varied imidacloprid concentrations in PBS pH 7.0 at the pulse amplitude of 0.15 V, the pulse width of 0.05 s, and the pulse period of 0.5 s. The inlay shows the calibration plot of peak currents ($-I_p$) *vs.* imidacloprid concentrations ([IMP]). The data points and error bars represent the mean values and standard deviation ($n = 3$), respectively.

### 3.9 Repeatability and reproducibility

The repeatability and reproducibility were tested for both within (intra) and between (inter) electrodes. The relative standard deviation (RSD) of the DPV peak currents of 0.40 mM IMP at a single MC/SPE was 3.42% ($n = 3$), indicating excellent repeatability within the electrode. The measurements of IMP at three different MC/SPEs yielded the RSD value of 2.23% ($n = 3$), demonstrating excellent reproducibility between electrodes.

### 3.10 Interference studies

The selectivity of the sensor was tested in the presence of potential interfering insecticides and ions including carbendazim, dichlorvos, ethion, indoxacarb, $Na^+$, $K^+$, $Ca^{2+}$, $Cl^-$, $Br^-$, $I^-$, and $SO_3^{2-}$.[44,52] The developed sensor was subjected to solutions containing 0.5 mM IMP in the absence or presence of 15-fold of the above-mentioned interferences. No significant change (<5%) in the peak currents was observed upon the addition of all the tested interferences, demonstrating excellent selectivity of the developed sensor toward IMP detection.

### 3.11 Applications to real samples

The validity of developed sensor was investigated by spiking and recovery tests (standard addition method) of IMP in various samples such as orange, lime, tomato, watermelon, tap water, and reservoir water. The results are shown as percentage recoveries in Table 2. The ~100% recoveries showed that the developed sensor has excellent tolerance to complex matrix interferences in all the tested samples and demonstrated high accuracy of the sensor in IMP detection.

### 3.12 Evaluation of washing solutions and temperatures in the removal of imidacloprid residues

Application of the developed sensor has been further extended to the evaluation of methods used in the removal of imidacloprid residues from fruit samples. In particular, the effects of washing solutions and temperatures were studied. Several washing solutions including tap water, 2% w/v NaCl, 5% w/v NaCl, 5% w/v bicarbonate, and a mixture of 5% w/v NaCl and

Table 2 Spike and recovery tests of IMP in orange, lime, tomato, watermelon, tab water, and reservoir water samples

| Sample | IMP added (mM) | IMP found (mM) | RSD (%) | Recovery (%) |
|---|---|---|---|---|
| Orange | 0.200 | 0.198 | 5.4 | 99.1 |
| Lime | 0.100 | 0.0962 | 3.8 | 96.2 |
| Tomato | 0.100 | 0.103 | 3.0 | 103.0 |
| Watermelon | 0.100 | 0.0981 | 4.3 | 98.1 |
| Tab water | 0.100 | 0.0972 | 2.9 | 97.2 |
| Reservoir water | 0.100 | 0.0980 | 3.8 | 98.0 |

Table 1 Comparison of electrochemical sensors for imidacloprid detection[a]

| Electrode | Method | Linear ranges (μM) | LOD (μM) | Samples | Ref. |
|---|---|---|---|---|---|
| GQDs/IL/MWCNTs/PANI/GCE | DPV | 0.030–12 | 0.009 | Apple, cucumber, and tomato | 44 |
| β-CD/rGO/GCE | DPV | 0.050–15.0<br>20–150 | 0.02 | — | 42 |
| Ag-Nafion/$TiO_2$-Nafion/GCE | DPV | 0.5–3.5 | 0.25 | Commercial imidacloprid sample and water sample | 45 |
| GO/GCE | SWV | 0.80–10 | 0.36 | Lake and tap water | 46 |
| MWCNTs-Nafion/GCE | DPV | 0.20–1.77 | 0.374 | Tap water, melon, and shrimp | 19 |
| MWCNTs/GCE | SWV | 0.24–3.50 | 0.415 | River water | 47 |
| β-CD/MWCNTs/MEA | DPV | 5.0–100 | 0.629 | Cabbage, cucumber, and tomato | 48 |
| Ag | SWV | 50–1000 | 6.90 | Tomato and orange | 49 |
| BDD | SWV | 30–200 | 8.60 | Plum juice | 50 |
| GCE | CV | 110–1900 | 30.0 | Potato | 51 |
| MC/SPE | DPV | 0.00–1000 | 2.54 | Orange, lime, tomato, watermelon, tap water, and reservoir water | This work |

[a] BDD: boron doped diamond, β-CD: β-cyclodextrin, CV: cyclic voltammetry, DPV: differential pulse voltammetry, GCE: glassy carbon electrode, GO: graphene oxide, GQDs: graphene quantum dots, IL: ionic liquid, MEA: microelectrode array, MWCNTs: multiwalled carbon nanotubes, PANI: polyaniline, rGO: reduce graphene oxide, and SWV: square wave voltammetry.

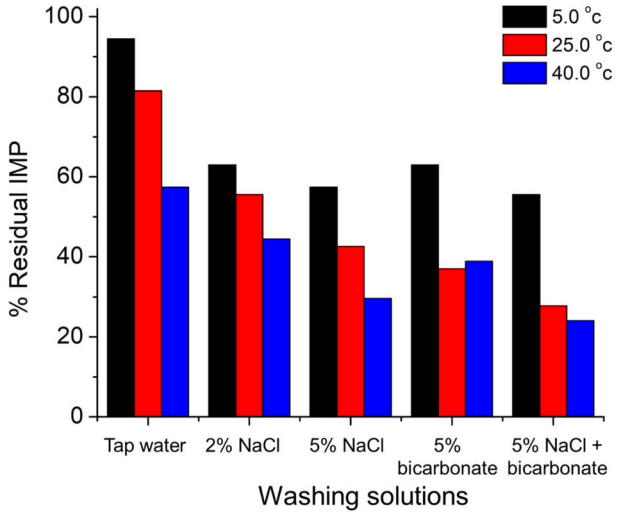


Fig. 10 % IMP residues in tomato samples after washing for 1 minute with different washing solutions at different temperatures.

5% w/v bicarbonate, which are readily available in supermarkets or grocery stores, were tested for their efficiencies in IMP removal. Three different washing temperatures (5 °C, 25 °C, and 40 °C) were also tested on tomato samples. In this work, tomatoes were chosen as the tested samples as they were often consumed without removing the peels.

The results which are presented in Fig. 10 show that washing tomatoes with the warm mixture of 5% w/v NaCl and 5% w/v bicarbonate at 40 °C can most efficiently remove the contaminated IMP in the sample due to the increase in IMP solubility at high temperatures.

## 4 Conclusions

This work has shown that the use of microporous carbon lowered the overpotential required in the cathodic detection of imidacloprid due to thin-layer diffusion within the porous structure. The increased electroactive surface area further enhanced the current responses and significantly improved the sensitivity of imidacloprid detection. The developed sensor showed excellent selectivity and limit of detection toward the determination of imidacloprid. The low-cost microporous carbon sensor has been further miniaturized *via* the use of disposable screen-printed electrodes for simple and convenient analysis using only *ca.* 50 μL of sample. The ~100% recovery showed that the sensor can be applied to various types of samples including orange, lime, tomato, watermelon, tap water, and reservoir water. Additionally, it has been demonstrated that the choice of washing solution and temperature plays a significant role in the removal of imidacloprid residues from fruits, providing valuable information for the food industry and households to ensure safety for consumers. Overall, this work has laid the foundation for the development of a cost-effective and versatile sensor for the detection of imidacloprid that can be applied to a wide range of applications such as environmental monitoring and food safety control.

## Author contributions

Keerakit Kaewket: investigation, writing – original draft, Kamonwad Ngamchuea: conceptualization, funding acquisition, resources, supervision, writing – review & editing.

## Conflicts of interest

The authors declare no known competing financial interests or personal relationships that could have appeared to influence the work reported in this paper.

## Acknowledgements

This work was supported by (i) Suranaree University of Technology (SUT), (ii) Thailand Science Research and Innovation (TSRI), and (iii) National Science, Research and Innovation Fund (NSRF) (Grant number: FF1-104-65-12-92(20)).

## References

1 D. Goulson, An overview of the environmental risks posed by neonicotinoid insecticides, *J. Appl. Ecol.*, 2013, **50**(4), 977–987.
2 T. E. Motaung, Chloronicotinyl insecticide imidacloprid: Agricultural relevance, pitfalls and emerging opportunities, *Crop Prot.*, 2020, **131**, 105097.
3 F. Wei, D. Wang, H. Li, P. Xia, Y. Ran and J. You, Toxicogenomics provides insights to toxicity pathways of neonicotinoids to aquatic insect, Chironomus dilutus, *Environ. Pollut.*, 2020, **260**, 114011.
4 Y. Li, L. Long, J. Ge, H. Li, M. Zhang, Q. Wan and X. Yu, Effect of imidacloprid uptake from contaminated soils on vegetable growth, *J. Agric. Food Chem.*, 2019, **67**(26), 7232–7242.
5 Y. Tao, F. Dong, J. Xu, D. Phung, Q. Liu, R. Li, X. Liu, X. Wu, M. He and Y. Zheng, Characteristics of neonicotinoid imidacloprid in urine following exposure of humans to orchards in China, *Environ. Int.*, 2019, **132**, 105079.
6 M. Ospina, L.-Y. Wong, S. E. Baker, A. B. Serafim, P. Morales-Agudelo and A. M. Calafat, Exposure to neonicotinoid insecticides in the US general population: Data from the 2015–2016 national health and nutrition examination survey, *Environ. Res.*, 2019, **176**, 108555.
7 F. Mohamed, I. Gawarammana, T. A. Robertson, M. S. Roberts, C. Palangasinghe, S. Zawahir, S. Jayamanne, J. Kandasamy, M. Eddleston and N. A. Buckley, Acute human self-poisoning with imidacloprid compound: a neonicotinoid insecticide, *PLoS One*, 2009, **4**(4), e5127.
8 S. Pang, Z. Lin, Y. Zhang, W. Zhang, N. Alansary, S. Mishra, P. Bhatt and S. Chen, Insights into the toxicity and degradation mechanisms of imidacloprid via physicochemical and microbial approaches, *Toxics*, 2020, **8**(3), 65.
9 L. G. Queiroz, C. C. A. do Prado, D. C. V. R. da Silva, L. E. T. Gomes, R. J. Marassi, É. C. Almeida, E. Pinto, F. T. da Silva and T. C. B. de Paiva, Ecological risk of

imidacloprid on the Brazilian non-target freshwater organisms Chironomus sancticaroli and Poecilia reticulata, *Environ. Monit. Assess.*, 2022, **194**(10), 1–14.

10 C. Blasco, M. Fernández, Y. Picó, G. Font and J. Mañes, Simultaneous determination of imidacloprid, carbendazim, methiocarb and hexythiazox in peaches and nectarines by liquid chromatography–mass spectrometry, *Anal. Chim. Acta*, 2002, **461**(1), 109–116.

11 A. Navalon, A. Gonzalez-Casado, R. El-Khattabi, J. L. Vilchez and A. R. Fernández-Alba, Determination of imidacloprid in vegetable samples by gas chromatography–mass spectrometry, *Analyst*, 1997, **122**(6), 579–581.

12 A. Vestri, M. Rippa, V. Marchesano, D. Sagnelli, G. Margheri, J. Zhou and L. Petti, LSPR immuno-sensing based on iso-Y nanopillars for highly sensitive and specific imidacloprid detection, *Environ. Monit. Assess.*, 2021, **9**(44), 9153–9161.

13 W. Xie, Y. Ju, J. Zhang, Y. Yang, Y. Zeng, H. Wang and L. Li, Highly sensitive and specific determination of imidacloprid pesticide by a novel Fe3O4@ SiO2@ MIPIL fluorescent sensor, *Anal. Chim. Acta*, 2022, **1195**, 339449.

14 M. A. Kamyabi and M. Moharramnezhad, Highly sensitive electrochemiluminescent insecticide sensor based on ZnO nanocrystals anchored nickel foam for determination of imidacloprid in real samples, *Electroanalysis*, 2020, **32**(5), 902–911.

15 J. Yang, L. Qi, J. A. Uqaili, D. Shi, L. Yin, Z. Liu, X. Tao, L. Dai and C. Lan, The terahertz metamaterial sensor for imidacloprid detection, *Int. J. RF Microw. Computer-Aided Eng.*, 2021, **31**(10), e22840.

16 X. Bi and K.-L. Yang, On-line monitoring imidacloprid and thiacloprid in celery juice using quartz crystal microbalance, *Anal. Chem.*, 2009, **81**(2), 527–532.

17 M. R. Majidi and S. Ghaderi, Facile fabrication and characterization of silver nanodendrimers supported by graphene nanosheets: A sensor for sensitive electrochemical determination of Imidacloprid, *J. Electroanal. Chem.*, 2017, **792**, 46–53.

18 M. A. Rashed, M. Faisal, S. Alsareii, M. Alsaiari, M. Jalalah and F. A. Harraz, Highly sensitive and selective electrochemical sensor for detecting imidacloprid pesticide using novel silver nanoparticles/mesoporous carbon/hematite ore ternary nanocomposite, *J. Environ. Chem. Eng.*, 2022, **10**(5), 108364.

19 E. E. Bruzaca, R. C. de Oliveira, M. S. Duarte, C. P. Sousa, S. Morais, A. N. Correia and P. de Lima-Neto, Electrochemical sensor based on multi-walled carbon nanotubes for imidacloprid determination, *Anal. Methods*, 2021, **13**(18), 2124–2136.

20 W. Si, W. Lei, Q. Hao, X. Xia, H. Zhang, J. Li, Q. Li and R. Cong, Facile synthesis of nitrogen-doped graphene derived from graphene oxide and vitamin B3 as high-performance sensor for imidacloprid determination, *Electrochim. Acta*, 2016, **212**, 784–790.

21 A. K. Tawade, D. Mohan Kumar, P. Talele, K. K. K. Sharma and S. N. Tayade, Flower-Like ZnO-Decorated Polyaniline–Graphene Oxide Nanocomposite for Electrochemical Oxidation of Imidacloprid: A Hybrid Nanocomposite Sensor, *J. Electron. Mater.*, 2019, **48**(12), 7747–7755.

22 A. E. F. Oliveira, G. B. Bettio and A. C. Pereira, Optimization of an Electrochemical Sensor for Determination of Imidacloprid Based on β-cyclodextrin Electropolymerization on Glassy Carbon Electrode, *Electroanalysis*, 2018, **30**(9), 1929–1937.

23 L. Zhao, J. Yang, H. Ye, F. Zhao and B. Zeng, Preparation of hydrophilic surface-imprinted ionic liquid polymer on multi-walled carbon nanotubes for the sensitive electrochemical determination of imidacloprid, *RSC Adv.*, 2017, **7**(8), 4704–4709.

24 S. El-Akaad, M. A. Mohamed, N. S. Abdelwahab, E. A. Abdelaleem, S. De Saeger and N. Beloglazova, Capacitive sensor based on molecularly imprinted polymers for detection of the insecticide imidacloprid in water, *Sci. Rep.*, 2020, **10**(1), 1–10.

25 L. Kong, X. Jiang, Y. Zeng, T. Zhou and G. Shi, Molecularly imprinted sensor based on electropolmerized poly (o-phenylenediamine) membranes at reduced graphene oxide modified electrode for imidacloprid determination, *Sens. Actuators, B*, 2013, **185**, 424–431.

26 W. Zhang, C. Liu, K. Han, X. Wei, Y. Xu, X. Zou, H. Zhang and Z. Chen, A signal on-off ratiometric electrochemical sensor coupled with a molecular imprinted polymer for selective and stable determination of imidacloprid, *Biosens. Bioelectron.*, 2020, **154**, 112091.

27 J. Ghodsi and A. A. Rafati, A novel molecularly imprinted sensor for imidacloprid pesticide based on poly (levodopa) electro-polymerized/TiO2 nanoparticles composite, *Anal. Bioanal. Chem.*, 2018, **410**(29), 7621–7633.

28 S. Li, C. Liu, G. Yin, J. Luo, Z. Zhang and Y. Xie, Supramolecular imprinted electrochemical sensor for the neonicotinoid insecticide imidacloprid based on double amplification by Pt-In catalytic nanoparticles and a Bromophenol blue doped molecularly imprinted film, *Microchim. Acta*, 2016, **183**(12), 3101–3109.

29 H. Shu, T. Lai, J. Ren, X. Cui, X. Tian, Z. Yang, X. Xiao and Y. Wang, Trimetallic metal-organic frameworks (Fe, Co, Ni-MOF) derived as efficient electrochemical determination for ultra-micro imidacloprid in vegetables, *Nanotechnology*, 2022, **33**(13), 135502.

30 Y. V. M. Reddy, J. H. Shin, J. Hwang, D.-H. Kweon, C.-H. Choi, K. Park, S.-K. Kim, G. Madhavi, H. Yi and J. P. Park, Fine-tuning of MXene-nickel oxide-reduced graphene oxide nanocomposite bioelectrode: Sensor for the detection of influenza virus and viral protein, *Biosens. Bioelectron.*, 2022, **214**, 114511.

31 Y. V. M. Reddy, J. H. Shin, V. N. Palakollu, B. Sravani, C.-H. Choi, K. Park, S.-K. Kim, G. Madhavi, J. P. Park and N. P. Shetti, Strategies, advances, and challenges associated with the use of graphene-based nanocomposites for electrochemical biosensors, *Adv. Colloid Interface Sci.*, 2022, 102664.

32 K. Kaewket, S. Maensiri and K. Ngamchuea, Adsorptive stripping voltammetry at microporous carbon: Determination and adsorption characteristics of

environmental contaminants, *Colloid Interface Sci. Commun.*, 2020, **38**, 100310.

33 T. Rattanaumpa, S. Maensiri and K. Ngamchuea, Microporous carbon in the selective electro-oxidation of molecular biomarkers: uric acid, ascorbic acid, and dopamine, *RSC Adv.*, 2022, **12**(29), 18709–18721.

34 R. G. Compton and C. E. Banks, *Understanding Voltammetry*, World Scientific, 2018.

35 M. C. Henstridge, E. J. Dickinson and R. Compton, Mass transport to and within porous electrodes. Linear sweep voltammetry and the effects of pore size: The prediction of double peaks for a single electrode process, *Russ. J. Electrochem.*, 2012, **48**(6), 629–635.

36 C. Punckt, M. A. Pope and I. A. Aksay, High selectivity of porous graphene electrodes solely due to transport and pore depletion effects, *J. Phys. Chem. C*, 2014, **118**(39), 22635–22642.

37 C. Batchelor-McAuley and R. G. Compton, Voltammetry of multi-electron electrode processes of organic species, *J. Electroanal. Chem.*, 2012, **669**, 73–81.

38 K. Ngamchuea, B. Tharat, P. Hirunsit and S. Suthirakun, Electrochemical oxidation of resorcinol: mechanistic insights from experimental and computational studies, *RSC Adv.*, 2020, **10**(47), 28454–28463.

39 R. G. Compton and C. E. Banks, *Understanding Voltammetry*, World Scientific, 2011.

40 S. A. Paula, O. A. E. Ferreira and P. A. César, Determination of imidacloprid based on the development of a glassy carbon electrode modified with reduced graphene oxide and manganese (ii) phthalocyanine, *Electroanalysis*, 2020, **32**(1), 86–94.

41 H. T. Chan, E. Kätelhön and R. G. Compton, Voltammetry using multiple cycles: Porous electrodes, *J. Electroanal. Chem.*, 2017, **799**, 126–133.

42 M. Chen, Y. Meng, W. Zhang, J. Zhou, J. Xie and G. Diao, β-Cyclodextrin polymer functionalized reduced-graphene oxide: Application for electrochemical determination imidacloprid, *Electrochim. Acta*, 2013, **108**, 1–9.

43 K. Ngamchuea, K. Tschulik, S. Eloul and R. G. Compton, In situ detection of particle aggregation on electrode surfaces, *ChemPhysChem*, 2015, **16**(11), 2338–2347.

44 P. Nasr-Esfahani, A. A. Ensafi and B. Rezaei, Fabrication of a highly sensitive and selective modified electrode for imidacloprid determination based on designed nanocomposite graphene quantum dots/ionic liquid/multiwall carbon nanotubes/polyaniline, *Sens. Actuators, B*, 2019, **296**, 126682.

45 A. Kumaravel and M. Chandrasekaran, Electrochemical determination of imidacloprid using nanosilver Nafion®/nanoTiO2 Nafion® composite modified glassy carbon electrode, *Sens. Actuators, B*, 2011, **158**(1), 319–326.

46 W. Lei, Z. Han, W. Si, Q. Hao, Y. Zhang, M. Xia and F. Wang, Sensitive and Selective Detection of Imidacloprid by Graphene-Oxide-Modified Glassy Carbon Electrode, *ChemElectroChem*, 2014, **1**(6), 1063–1067.

47 W. D. A. Paiva, T. M. B. Oliveira, C. P. Sousa, P. de Lima Neto, A. N. Correia, S. Morais, D. R. Silva and S. S. L. Castro, Electroanalysis of imidacloprid insecticide in river waters using functionalized multi-walled carbon nanotubes modified glassy carbon electrode, *J. Electrochem. Soc.*, 2018, **165**(10), B431.

48 W. Zhang, C. Liu, X. Zou, H. Zhang and Y. Xu, A β-CD/MWCNT-modified-microelectrode array for rapid determination of imidacloprid in vegetables, *Food Anal. Methods*, 2019, **12**(10), 2326–2333.

49 N. Ajermoun, S. Aghris, A. Farahi, S. Lahrich, S. Saqrane, M. Bakasse and M. A. El Mhammedi, Electrochemical reduction of neonicotinoids insecticides catalysed by metallic silver: case of the detection of imidacloprid in tomato and orange juices, *Int. J. Environ. Anal. Chem.*, 2021, **101**(5), 585–597.

50 M. B. Brahim, H. B. Ammar, R. Abdelhédi and Y. Samet, Electrochemical behavior and analytical detection of Imidacloprid insecticide on a BDD electrode using square-wave voltammetric method, *Chin. Chem. Lett.*, 2016, **27**(5), 666–672.

51 V. J. Guzsvány, F. F. Gaál, L. J. Bjelica and S. N. Ökrész, Voltammetric determination of imidacloprid and thiamethoxam, *J. Serb. Chem. Soc.*, 2005, **70**(5), 735–743.

52 R. R. Gioia, J. O. Fernandes, C. A. R. Bernardino, C. F. Mahler, B. F. Braz, C. S. C. Lopes, B. S. Archanjo, E. S. Ribeiro, E. D'Elia and R. E. Santelli, An electrochemical sensor-based carbon black associated with a modified mixed oxide (SiO2/TiO2/Sb2O5) for direct determination of thiamethoxam in raw honey and water samples, *Microchim. Acta*, 2022, **189**(8), 1–10.